Microwave-assisted synthesis of 2,5-dioxo-pyrano[3,2-*c*] quinoline-3-carboxylates and their investigation as antiproliferative agents targeting EGFR and/or BRAF^{V600E}

Ashraf A. Aly[1] · Hisham A. Abd El-Naby[1] · Essam Kh. Ahmed[1] · Raafat M. Shaker[1] · Sageda A. Gedamy[1] ·
Bahaa G. M. Youssif[2] · Hesham A. M. Gomaa[3] · Olaf Fuhr[4] · Alan B. Brown[5] · Mahmoud A. A. Ibrahim[1,6] ·
Lamiaa E. Abd El-Haleem[1]

Abstract

Pyrano[3,2-*c*]quinoline-3-carboxylate derivatives **3a-j** were synthesized efficiently by the microwave–irradiated condensa-tion of 4-hydroxy-2-oxo-1,2-dihydroquinoline-3-carbaldehydes **4a-j** with ethyl cyanoacetate (**2**) in the presence of ethanol and a catalytic amount of piperidine. The structures of the products were confirmed by a combination of spectral techniques including infra-red (IR), nuclear magnetic resonance (NMR), mass spectrometry (MS) and elemental analyses in addition to X-ray structure analysis. The synthesized compounds **3a-j** were tested for their in vitro antiproliferative activity against four human cancer cell lines using the MTT assay and doxorubicin as the reference drug: pancreas (Panc-1) cancer cell line, breast cancer (MCF-7) cell line, colon cancer (HT-29) cell line, and epithelial cancer (A-549) cell line. In comparison to the standard doxorubicin ($GI_{50} = 1.10$ μM), compounds **3a-j** demonstrated promising antiproliferative action, with GI_{50} values ranging from 1.30 to 5.90 μM. The most effective derivatives were compounds **3c**, **3g**, **3h**, and **3i** with GI_{50} values ranging from 1.30 to 2.20 μM. The most potent antiproliferative derivative, compound **3c** ($R^1 = OCH_3$, $R^2 = R^3 = H$), was also the most potent EGFR inhibitor, with an IC_{50} value of 105 ± 08 nM, 1.3-fold less potent than erlotinib ($IC_{50} = 80 \pm 05$ nM). Compounds **3g** ($R^1 = Br$, $R^2 = R^3 = H$) and **3h** ($R^1 = Cl$, $R^2 = R^3 = H$) were the second and third most active, with IC_{50} values of 124 ± 10 nM and 195 ± 13 nM, respectively. Molecular docking calculations were conducted to inspect the docking scores and poses of the most promising compounds against EGFR and BRAF^{V600E}. Based on the docking computations, compounds **3c** and **3g** revealed promising docking scores against the EGFR and BRAF^{V600E} with values of -7.9 and -8.3 kcal/mol, respectively.

✉ Ashraf A. Aly
ashrafaly63@yahoo.com; ashraf.shehata@mu.edu.eg

Hisham A. Abd El-Naby
hisham_minia@mu.edu.eg

Essam Kh. Ahmed
essam.mohd@mu.edu.eg

Raafat M. Shaker
rshaker63@mu.edu.eg

Sageda A. Gedamy
sagedaali332@yahoo.com

Bahaa G. M. Youssif
bgyoussif2@gmail.com

Hesham A. M. Gomaa
hasoliman@ju.edu.sa

Olaf Fuhr
olaf.fuhr@kit.edu

Alan B. Brown
abrown@fit.edu

Mahmoud A. A. Ibrahim
m.ibrahim@compchem.net

Lamiaa E. Abd El-Haleem
lamiaaelsayed2013@yahoo.com

Chemistry Department, Faculty of Science, Minia University, El-Minia 61519, Egypt

[2] Pharmaceutical Organic Chemistry Department, Faculty of Pharmacy, Assiut University, Assiut 71526, Egypt

[3] Department of Pharmacology, College of Pharmacy, Jouf University, 72341 Sakaka, Aljouf, Saudi Arabia

Institute of Nanotechnology (INT) and Karlsruhe Nano Micro Facility (KNMFi), Karlsruhe Institute of Technology (KIT), Kaiserstraße 12, 76131 Karlsruhe, Germany

[5] Department of Chemistry and Chemical Engineering, Florida Institute of Technology, Melbourne, FL, USA

[6] School of Health Sciences, University of KwaZulu-Natal, Westville Campus, Durban 4000, South Africa

Graphical Abstract
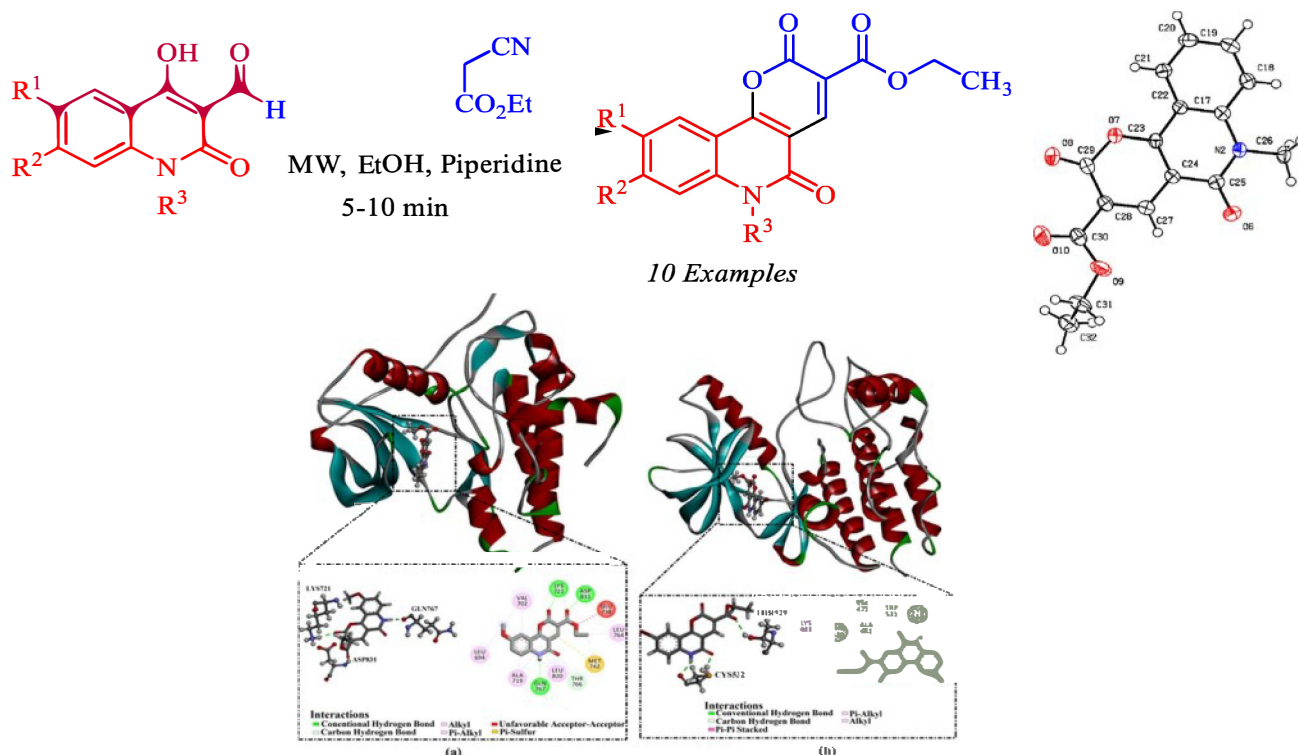
10 Examples

Introduction

Synthesis of heterocycles has become very important and their synthetic tools has become the subject of hundreds of articles due to their wide applications. Accordingly catalytic approach as a type of green chemistry has been utilized to facilitate the synthesis of heterocycles (Bibak and Poursattar Marjani 2023; Beigiazaraghbelagh and Poursattar Marjani 2024; Poursattar Marjani et al. 2023; Maynard 2005; Safari et al. 2023). Moreover, functionalized heterocycles have great importance because they have been used as building blocks in pharmaceutical and industrial applications (Win et al. 2019). Pyranoquinolinones and their derivatives possess a wide range of biological activities including anticancer (Saeed et al. 2020; Upadhyay et al. 2023; Ramadan et al. 2021) anti-tumor (Upadhyay et al. 2018), anti-inflammatory (Ramadan et al. 2021), antibacterial- (Insuasty et al. 2019; Moynihan et al. 2022), antifungal- (Di Liberto et al. 2020) and anti-platelet activities (Prasad et al. 2017), as well as nitric oxide production (Ito et al. 2004). Pyrano[3,2-*c*]quinolones are also widely available in bioactive natural products, and

analogs exhibit diversified biological activities depending on the structure type in a therapeutic context (Magedov et al. 2008) (Fig. 1). For example, Zanthosimuline (**A**), isolated from *Zanthoxylum simulans,* was reported as an anticancer agent having activity against multidrug-resistant KB-VI cancer cells (Chen et al. 1994). In addition, *N*-methylflindersine (**B**) isolated from *Toddalia asiatica* exhibits antimicrobial and antifungal activity (Duraipandiyan Ignacimuthu, 2009), whereas haplamine (**C**) isolated from *Haplophyllum villosum* displays good anticancer activity (Fig. 1) (Al-Yahya et al. 1992). Haplamine (**C**) was found active against the HCT-116 line, and showed significant cytotoxic activity against all the tested cell lines (Ea et al. 2008).

Interstingly, a catalytic synthetic approach of various pyrano[3,2-*c*]quinolone and their similar compounds was reported. (Aghbash et al. 2018, Aghbash and Pesyan 2022, Aghbash et al. 2019, Pesyan et al. 2020).

Recently, we synthesized quinolone and pyranoquinolone derivatives that have shown various biological activities such as those against urease (Elshaier et al. 2022; Elbastawesy et al. 2021) non-ATP competitive Src kinase (Ramadan et al. 2021), proliferative EGFR-TK (Elbastawesy et al. 2019),

Zanthosimuline (**A**) *N*-methylflindersine (**B**) Haplamine (**C**)

potential apoptotic antiproliferative activity (Ramadan et al. 2020) and of ERK with efficacy in BRAF-mutant Melanoma (Aly et al. 2019).

Microwave-assisted organic synthesis (MAOS) is superior to the conventional method of heating in many contexts (Badiger et al. 2022; Kappe 2004; Kalla and Devaraju, 2017). Organic chemists have discovered the advantage of microwaves to fast and uniformly heat organic reaction mixtures in a synthetic process (Ohlsson and Bengtsson 2001).

Previously, quinolones **1a,b** reacted with ethyl 2-cyano-3-ethoxyacrylate (**2**) to give pyrano[3,2-*c*]quinolones **3a,b** (Schmidt and Junek 1978; Morsy et al. 2016). Similarly, the reaction of 4-hydroxy-1-methyl-2-oxo-1,2-dihydroquinoline-3-carbaldehyde (**4b**) with diethyl malonate (**5**) in acetic anhydride Ac₂O/Et₃N mixture afforded **3b** in 80% yield (Buckle et al. 1975) (Scheme 1).

It was reported that acquired BRAF^{V600E} mutation has a significant for the resistance mechanism following therapy with EGFR inhibitors (Ho et al. 2017). The feedback activation of EGFR signaling is also linked to the emergence of resistance in colorectal cancer (Hyman et al. 2015). It was reported that the BRAF-EGFR combination has also a remarkable therapeutic effect in people with metastatic colorectal cancer who have the BRAF^{V600E} mutation (Ho et al. 2017). As a result, inhibiting the two kinases sequentially may be responsible for the issue of EGFR activation (Ho et al. 2017).

Using microwave irradiation, we herein synthesized pyrano[3,2-*c*]quinoline-3-carboxylates **3a-j** more quickly, efficiently, cleanly as well as economically. The new series of hybrids will be also tested as an antiproliferative agent against a panel of four cancer cell lines. Furthermore, the most active compounds were tested against EGFR and BRAF^{V600E} as potential targets for antiproliferative activity. Using an MTT assay, the compounds were tested on a panel of four different cancer cell lines. The EGFR and BRAF enzymatic assays were used to investigate the hybrids' potential antiproliferative mechanism. The docking poses and scores of the most promising compounds were anticipated against the EGFR and BRAF^{V600E} targets. The current findings draw attention to compounds **3c** and **3g** as promising options for treating cancer disease.

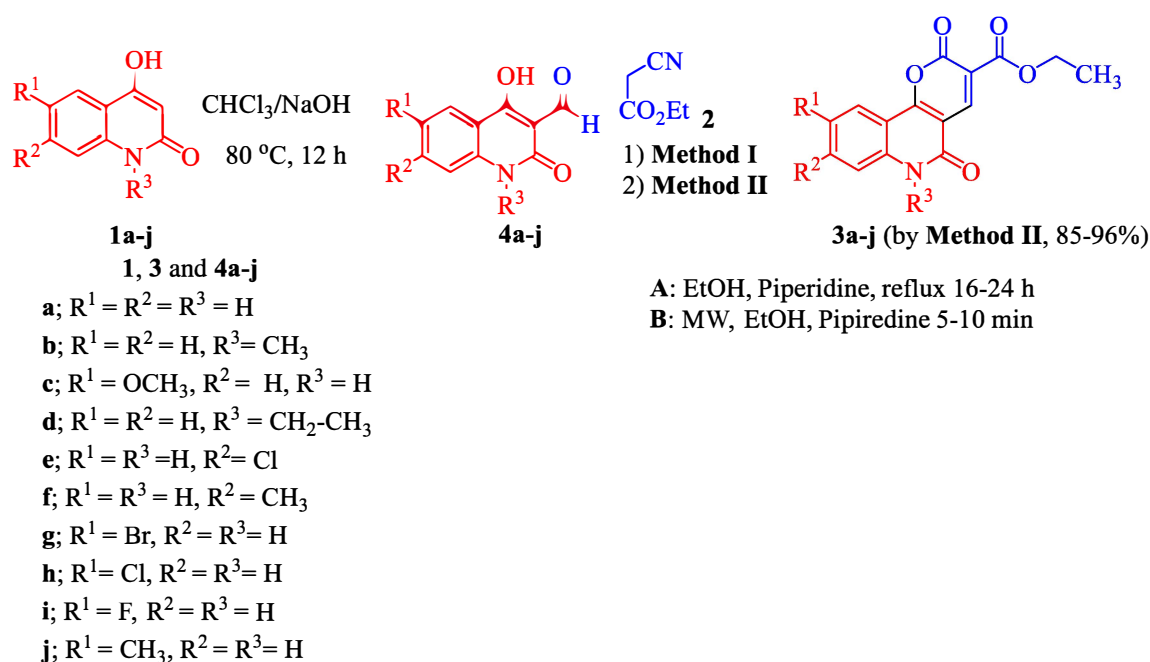## Results and dicussion

Chemistry

Pyrano[3,2-*c*]quinoline-3-carboxylate derivatives **3a-j** were obtained as single products from the reaction of the prepared 4-hydroxy-2-oxo-quinoline-3-carbaldehydes **4a–j** with ethyl cyanoacetate (**2**) (Scheme 2). The reaction was performed under different conditions, such as: ethanol/

1a,b

1a, R = H; **1b;** R = CH₃

2

1) NaOEt/EtOH

reflux, 2) HCl

3a,b (75-79%)

4b

5

Et₃N/Ac₂O

reflux

3b (80%)

R^1, R^2 with OH on quinolinone. CHCl$_3$/NaOH, 80 °C, 12 h → 4a-j. CN, CO$_2$Et **2**; 1) **Method I** 2) **Method II** → **3a-j** (by **Method II**, 85-96%)

1a-j   **4a-j**

1, 3 and **4a-j**

a; R^1 = R^2 = R^3 = H
b; R^1 = R^2 = H, R^3 = CH$_3$
c; R^1 = OCH$_3$, R^2 = H, R^3 = H
d; R^1 = R^2 = H, R^3 = CH$_2$-CH$_3$
e; R^1 = R^3 = H, R^2 = Cl
f; R^1 = R^3 = H, R^2 = CH$_3$
g; R^1 = Br, R^2 = R^3 = H
h; R^1 = Cl, R^2 = R^3 = H
i; R^1 = F, R^2 = R^3 = H
j; R^1 = CH$_3$, R^2 = R^3 = H

A: EtOH, Piperidine, reflux 16-24 h
B: MW, EtOH, Pipiredine 5-10 min

Scheme 2 Synthesis of pyrano[3,2-*c*]quinoline-3- carboxylates **3a-j**

Table 1 Synthesis of pyrano[2,3-**c**]quinolones **3a-j** by **Methods I** and **II**

Compounds	Time (min or h)		Yield (%)	
	Method I (h)	Method II (min)	Method I	Method II
3a	16	5	75	85
3b	18	5	65	88
3c	16	5	77	87
3d	24	10	80	86
3e	22	6	78	94
3f	24	10	80	87
3g	26	10	64	96
3h	20	5	65	94
3i	22	7	82	92
3j	20	6	67	87

piperidine at reflux (**Method I**) or ethanol/piperidine/ Microwave (**Method II**) (Scheme 2).

Noticeably, when the reaction was carried out by **Method II**, the yields of the products **3a-j** were obtained in the best yields (85–96%) and also took a shorter time (Table 1).

Method II showed that the reaction between **4a-j** and **2** was completed faster and gave excellent yields compared with the conventional method (**Method I**). Under microwave irradiation, compounds **3a**, **3b** and **3c** were formed completely in a lesser time (> 5 min) and afforded the yields of 85%, 88% and 87%, respectively. The best yield was obtained in the case of **3g** (96%) and the reaction was completed in 10 min (Table 1).

The structure of the obtained products of **3a–j** was confirmed by IR, NMR, and mass spectra, in addition to elemental analysis. Mass spectroscopy and elemental analysis of **3c** proved its chemical formula as $C_{16}H_{13}NO_6$. IR spectrum of **3c** showed absorption bands at $\nu_{max} = 3276, 3076, 1766, 1671$ and 1604 cm^{-1} for NH, CH-Ar, CO-pyranone, CO-ester and CO-quinolone groups, respectively. The ^{1}H NMR spectrum revealed two singlets at $\delta_H = 12.16$ (1H, NH), and 3.87 (3H, CH$_3$O). The ethyl protons resonated as a quartet and a triplet at $\delta_H = 4.30$ ($J = 7.1$ Hz, CH$_2$) and 1.32 ppm ($J = 7.1$ Hz, CH$_3$). The ^{13}C NMR spectrum of **3c** supported the ^{1}H NMR spectral data by the appearance of six distinctive carbon signals at $\delta_C = 161.9$ (C=O, pyranone), 161.4 (C=O, ester), 158.3 (C=O, quinolone), 61.2 (CH$_2$–ester), 55.7 (OCH$_3$) and 14.0 (CH$_3$–ester), respectively.

Mass spectroscopy and elemental analysis of **3h** confirmed its molecular formula as $C_{15}H_{10}ClNO_5$. The IR spectrum of **3h** revealed absorption bands at $\nu = 3270, 3058, 2891, 1769, 1690$ and 1660 cm^{-1} corresponding to NH, CH–Aromatic, CH–Aliphatic, carbonyl-pyranone, carbonyl-ester and carbonyl-quinolone, respectively. Figure 2 illustrates the NMR spectroscopic data of compound **3h**. The ^{1}H NMR spectrum showed the ester protons as a quartet at $\delta_H = 4.30$ ($J = 7.1$ Hz, CH$_2$) and a triplet at $\delta_H = 1.32$ ($J = 7.1$ Hz, CH$_3$) (see the Experimental). In **3h**, the CH–Pyranone carbon signal appeared at $\delta_C = 145.2$. In addition, the CH$_2$ and CH$_3$ of the ethyl group resonated at $\delta_C = 61.4$ and 14.0, respectively. Finally, the structure of

Fig. 2 ^{1}H NMR and ^{13}C NMR spectral data some distinctive protons and carbons of compound **3h**
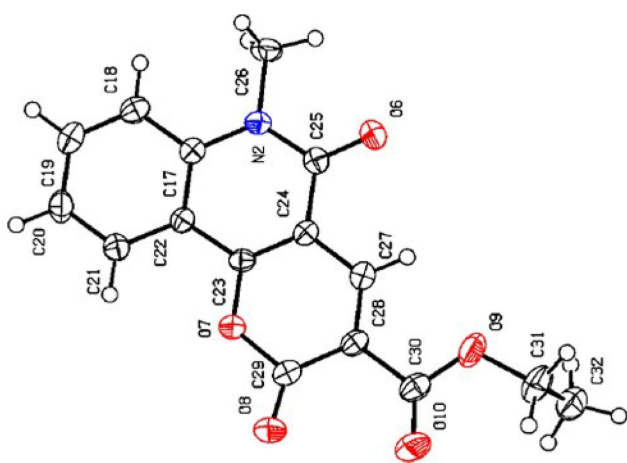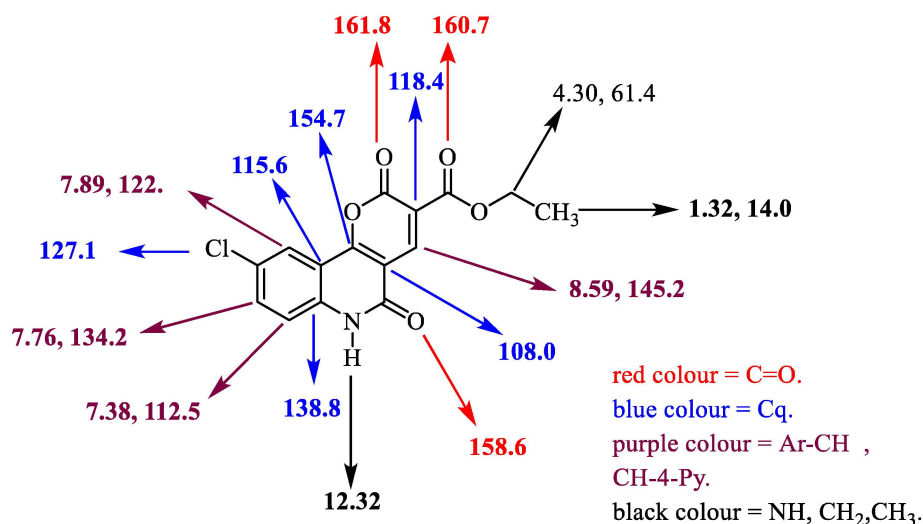

161.8   160.7
118.4
154.7
115.6
7.89, 122.
127.1 ← Cl
7.76, 134.2
7.38, 112.5   138.8
12.32
4.30, 61.4
CH₃ → 1.32, 14.0
8.59, 145.2
108.0
158.6

red colour = C=O.
blue colour = Cq.
purple colour = Ar-CH , CH-4-Py.
black colour = NH, CH₂,CH₃.

Fig. 3 Molecular structure of compound **3b** identified according to IUPAC nomenclature as ethyl 6-methyl-2,5-dioxo-5,6-dihydro-2H-pyrano[3,2-c]quinoline-3-carboxylate

pyrano[2,3-c]quinolones was proved by X-ray structure analysis as shown for compound **3b** (Fig. 3), which is consistent with the spectroscopic analysis of other derivatives.

The mechanism proposed for formation of compounds **3a-j** begins with nucleophilic attack of the active anion formed from **2** to the electrophilic carbonyl in **1a-j** to give intermediates **6a-j** (Scheme 3). Further nucleophilic attack of the hydroxyl-lone pair would then occur to the electrophilic nitrile to form intermediate **7a-j** (Scheme 2). Elimination of water from **7a-j** would give intermediate **8a-j**. Finally, hydrolysis of the imino group would give **3a-j** (Scheme 3).

Biology

Cell viability assay

The human mammary gland epithelial (MCF-10A) cell line was employed (Youssif et al. 2019; Mahmoud et al. 2022) to assess the viability of **3a-j**. MCF-10A cells were treated

Scheme 3 Mechanism describes the formation of compounds **3a-j**
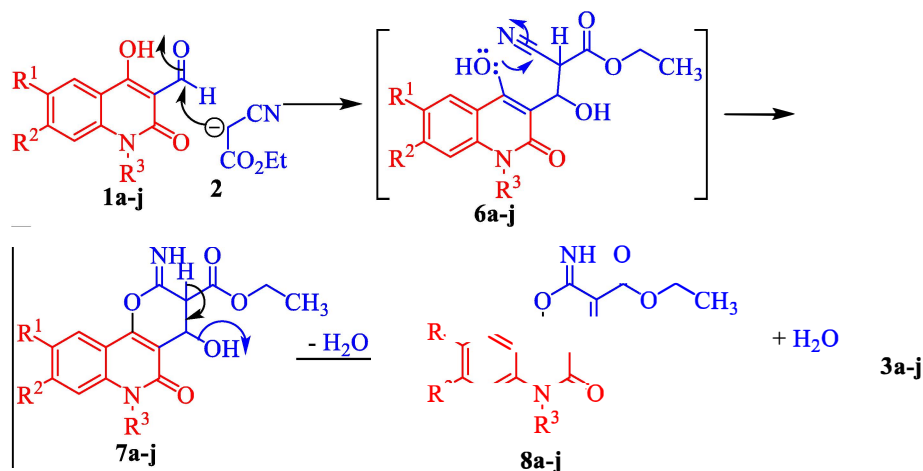
for four days with compounds **3a-j** before being evaluated for viability using the MTT assay. Table 2 demonstrates that none of the chemicals tested displayed cytotoxic effects, and cell viability at 50 μM was greater than 88%.

Antiproliferative activity

Compounds **3a-j** were tested for antiproliferative activity against four human cancer cell lines using the MTT assay (El-Sherief et al. 2018; Abdelrahman et al. 2017) and doxorubicin as the reference drug: pancreas (Panc-1) cancer cell line, breast cancer (MCF-7) cell line, colon cancer (HT-29) cell line, and epithelial cancer (A-549) cell line. Table 2 shows the median inhibitory concentration (IC_{50}) along with average IC_{50} (GI_{50}). In comparison to the standard doxorubicin ($GI_{50} = 1.10$ μM), **3a-j** demonstrated promising antiproliferative action, with GI_{50} values ranging from 1.30 to 5.90 μM. The most effective derivatives were compounds **3c**, **3g**, **3h**, and **3i**, with GI_{50} values ranging from 1.30 to 2.20 μM.

The methoxy derivative compound **3c** ($R^1 = OCH_3$, $R^2 = R^3 = H$) was the most potent derivative of all synthesized compounds, with a GI_{50} value of 1.30 μM, comparable to standard doxorubicin's GI_{50} value of 1.10 μM. Replacement of the methoxy group in position nine of compound **3c** with halogen atoms as in compounds **3g** ($R^1 = Br$, $R^2 = R^3 = H$), **3h** ($R^1 = Cl$, $R^2 = R^3 = H$) and **3i** ($R^1 = F$, $R^2 = R^3 = H$) resulted in a marketed decrease in antiproliferative action, with GI_{50} values of 1.65, 1.80, and 2.20 μM, respectively, being 1.3-fold, 1.4-fold, and 1.7-fold less potent than **3c**, respectively.

Similarly, replacing the methoxy group in **3c** with a methyl group as in compound **3j** ($R^1 = CH_3$, $R^2 = R^3 = H$) or by hydrogen atom as in compound **3a** ($R^1 = H$, $R^2 = R^3 = H$) resulted in a decrease in antiproliferative activity with GI_{50} values of 3.40 μM and 4.70 μM, respectively, being 2.6-fold

and 3.6-fold less potent than **3c**. These findings indicated the importance of the position nine substitution pattern on the antiproliferative activity of the newly synthesized compounds, and that activity increased in the following order: $OCH_3 > Br > Cl > F > CH_3 > H$.

The nitrogen atom of the quinoline ring moiety is another component that may be essential in the activity of the tested compounds. The GI_{50} value of compound **3a** ($R^1 = R^2 = H$, $R^3 = H$) with a free nitrogen atom in the quinoline moiety was 4.70 μM. Substitution of the nitrogen atom by a methyl group as in compound **3b** ($R^1 = H$, $R^2 = R^3 = CH_3$) or ethyl group as in compound **3d** ($R^1 = H$, $R^2 = R^3 = CH_3CH_2$) resulted in less potent compounds with GI_{50} values of 5.90 μM and 5.40 μM, respectively. Compounds **3b** and **3d** were the least potent derivatives, suggesting the relevance of the quinoline ring's free nitrogen atom for antiproliferative activity.

Assay for EGFR inhibitory activity

Compounds **3c**, **3g**, and **3h**, the most potent antiproliferative derivatives, were studied as potential EGFR inhibitors as a possible molecular target for their activity (Mohamed et al. 2021). In Table 3, data were presented as IC_{50} values versus erlotinib as a reference drug. In comparison to erlotinib ($IC_{50} = 80$ nM), the investigated compounds had good EGFR inhibitory effect, with IC_{50} values ranging from 105 to 195 nM. In all cases, the investigated compounds were less powerful than the reference erlotinib.

The most potent antiproliferative derivative, compound **3c** ($R^1 = OCH_3$, $R^2 = R^3 = H$), was also the most potent EGFR inhibitor, with an IC_{50} value of 105 ± 08 nM, 1.3-fold less potent than erlotinib ($IC_{50} = 80 \pm 05$ nM). Compounds **3g** and **3h** were the second and third most active, with IC_{50} values of 124 ± 10 nM and 195 ± 13 nM, respectively. These findings suggest that EGFR may be a possible target for the

Table 2 IC_{50} of compounds **3a-j** against four cancer cell lines using Doxorubicin as a reference

Compound	Cell viability%	Antiproliferative activity $IC_{50} \pm$ SEM (μM)				
		A-549	MCF-7	Panc-1	HT-29	Average IC_{50} (GI_{50})
3a	89	4.70 ± 0.40	4.50 ± 0.40	4.80 ± 0.40	4.90 ± 0.40	4.70
3b	89	5.70 ± 0.50	5.60 ± 0.50	5.90 ± 0.50	6.00 ± 0.50	5.90
3c	91	1.30 ± 0.10	1.10 ± 0.10	1.40 ± 0.10	1.40 ± 0.10	1.30
3d	87	5.30 ± 0.50	5.10 ± 0.50	5.60 ± 0.50	5.60 ± 0.50	5.40
3e	92	2.60 ± 0.20	2.40 ± 0.20	2.90 ± 0.20	2.90 ± 0.20	2.70
3f	90	4.00 ± 0.40	3.90 ± 0.30	4.10 ± 0.40	4.20 ± 0.40	4.00
3g	91	1.60 ± 0.10	1.40 ± 0.10	1.80 ± 0.10	1.80 ± 0.10	1.65
3h	90	1.80 ± 0.10	1.50 ± 0.10	1.90 ± 0.10	1.90 ± 0.10	1.80
3i	88	2.10 ± 0.20	1.90 ± 0.10	2.40 ± 0.20	2.40 ± 0.20	2.20
3j	90	3.40 ± 0.30	3.00 ± 0.20	3.50 ± 0.30	3.70 ± 0.30	3.40
Doxorubicin		1.40 ± 0.08	0.90 ± 0.02	1.00 ± 0.02	1.20 ± 0.03	1.10

Table 3 IC$_{50}$ of compounds **3c**, **3g** and **3h** against EGFR and BRAF^{V600E}

Compd	EGFR inhibition IC$_{50}$±SEM (nM)	BRAF^{V600E} inhibition IC$_{50}$±SEM (nM)
3c	105±08	133±10
3g	124±10	125±09
3h	195±13	217±15
Erlotinib	80±05	60±05

compounds studied, which require structural modifications to provide more potent variants.

Assay for mutant BRAF

The most effective antiproliferative derivatives, compounds **3c**, **3g**, and **3h**, were examined further as potential BRAF^{V600E} inhibitors as a probable molecular target for their activity (Mohassab et al. 2021).

Table 3 displays data as IC$_{50}$ values vs erlotinib as a reference medication. The investigated compounds inhibited BRAF^{V600E} with IC$_{50}$ values ranging from 125 to 217 nM, being at least twofold less effective than erlotinib (IC$_{50}$ = 60 ± 5 nM). These findings indicate that BRAF^{V600E} may not be an optimal target for the compounds under consideration.

Molecular docking

The docking scores and poses of the most promising compounds –namely, **3c**, **3g**, and **3h** against the EGFR and BRAF^{V600E} were predicted utilizing AutoDock 4.2.6 software. The predicted binding scores and conventional H-bonds of the investigated compounds against the EGFR and BRAF^{V600E} are compiled in Table 4. From Table 4, all investigated compounds demonstrated satisfactory docking scores against EGFR and BRAF^{V600E} with values in the range of −6.9 to −7.9 kcal/mol and −7.7 to −8.3 kcal/mol, respectively. The outstanding binding scores of the investigated compounds may be imputed to their capability of forming H-bonds, hydrophobic, pi-based, and vdW interactions with the binding pockets of the investigated targets.

As data registered in Table 4, compounds **3c** and **3g** exhibited eminent docking scores with values of −7.9 and −8.3 kcal/mol towards EGFR and BRAF^{V600E}, respectively. Investigating the docking pose of compound **3c** inside the binding pocket of the EGFR demonstrated that compound **3c** formed H-bonds with LYS721 (2.18 Å), GLN767 (2.09 Å), and ASP831 (2.08 Å). Besides, compound **3c** established pi-sulfur interaction with MET742 and C–H-bond with ASP831 (Fig. 4). On the other hand, compound **3g** established three H-bonds with the binding pocket of BRAF^{V600E} with THR529 (2.26 Å), and CYS532 (1.63, 2.06 Å). Besides, compound **3g** demonstrated pi-pi stacking and C–H–bond interaction with TRP531 of BRAF^{V600E} (Fig. 4).

Erlotinib, a positive control, unveiled favorable binding scores against EGFR and BRAF^{V600E} with values of −8.6 and −8.4 kcal/mol, respectively (Table 4). As listed in Table 4, erlotinib exhibited two H–bonds with MET769 (1.62 Å) and CYS773 (1.91 Å) of EGFR and THR529 (2.07 Å) and CYS532 (2.02 Å) of BRAF^{V600E}.

Experimental

Chemistry

Melting points were taken in open capillaries on a Gallenkamp melting point apparatus (Weiss–Gallenkamp, Loughborough, UK) and are uncorrected. The IR spectra were recorded by the ATR technique (ATR = Attenuated Total Reflection) with a FT device (FT-IR Bruker IFS 88), Institute

Table 4 Computed binding scores (in kcal/mol) and conventional H-bonds for the most potent compounds against EGFR and BRAF^{V600E}

| Compound name	EGFR		BRAF^{V600E}	
	Docking scores (kcal/mol)	Conventional H-bond	Docking scores (kcal/mol)	Conventional H-bond
3c	−7.9	LYS721 (2.18 Å) GLN767 (2.09 Å) ASP831 (2.08 Å)	−8.1	SER536 (2.55 Å) CYS532 (1.93, 1.80 Å)
3g	−7.5	THR752 (2.26 Å) CYS755 (2.06, 1.63 Å)	−8.3	THR529 (2.26 Å CYS532 (1.63, 2.08 Å)
3h	−7.3	LYS721 (2.16 Å) GLN767 (2.17 Å) ASP831 (2.17 Å)	−7.9	THR529 (2.16 Å) CYS532 (1.63, 2.08 Å)
Erlotinib	−8.6	MET769 (1.62 Å) CYS773 (1.91 Å)	−8.4	THR529 (2.07 Å) CYS532 (2.02 Å)
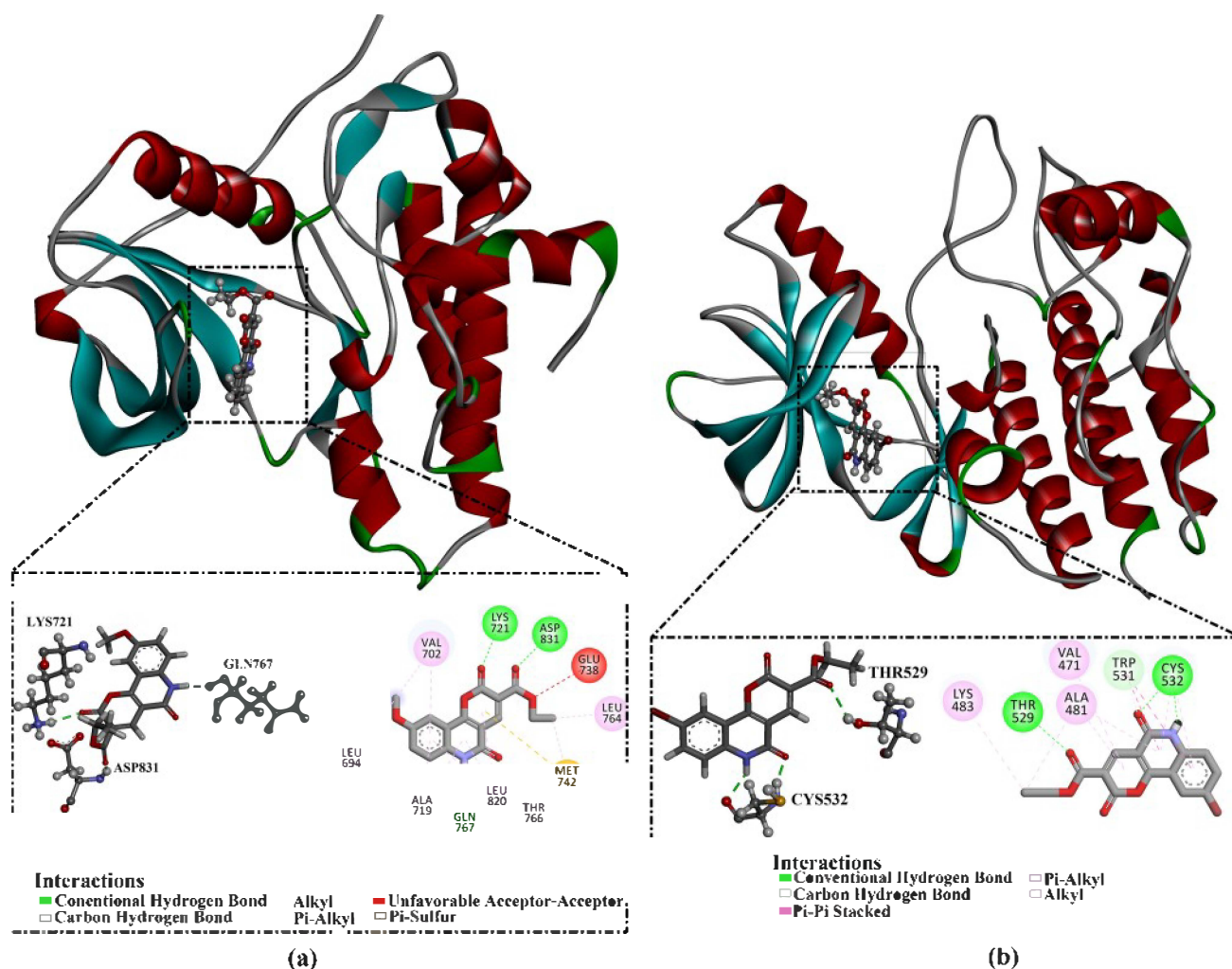
Fig. 4 3D and 2D representations of (**a**) compound **3c** inside the binding pocket of EGFR (PDB ID: 1M17) and (**b**) compound **3g** within the binding pocket of BRAF^V600E (PDB ID: 3OG7). Green color indicates H-bonds; light green color indicates C–H bonds; pink color represents alkyl and pi-alkyl interactions; purple color refers to pi–pi stacked interactions; the red color indicates unfavorable interactions; and yellow color represents pi-sulfur interactions

of Organic Chemistry, Karlsruhe University, Karlsruhe, Germany. The NMR spectra were measured in DMSO-d_6 on a Bruker AV-400 spectrometer, 400 MHz for ^{1}H, and 100 MHz for ^{13}C; and the chemical shifts are expressed in δ (ppm), versus internal tetramethylsilane (TMS) = 0 for ^{1}H and ^{13}C. The description of signals includes: s = singlet, d = doublet, dd = doublet of doublet, t = triplet, q = quartet, and m = multiplet. The following abbreviations were used to distinguish between signals: Ar–H = aromatic–CH. Signals of the ^{13}C NMR spectra were assigned with the help of DEPT90 and DEPT135 and were specified in the following way: + = primary or tertiary carbon atoms (positive DEPT signal), − = secondary carbon atoms (negative DEPT signal), C_q = quaternary carbon atoms (no DEPT signal). Correlations were established using ^{1}H–^{1}H COSY, and ^{1}H–^{13}C HSQC and HMBC experiments. Mass spectra were recorded on a FAB (fast atom bombardment) Thermo Finnigan Mat 95 (70 eV). Elemental analyses were carried out at the Microanalytical Center, Cairo University, Egypt. TLC was performed on analytical Merck 9385 silica aluminum sheets (Kieselgel 60) with Pf254 indicator; TLC's were viewed at λ_{max} = 254 nm.

Starting materials

1,6-Disubstituted-quinoline-2,4-(1H,3H)-diones **1a–j** were prepared according to the literature (Bhudevi et al. 2009). 4-Hydroxy-2,5-dioxo-1,2-dihydroquinoline-3-carbaldehydes **4a-j** were synthesized according to the literature (Bhudevi et al. 2009; Mohamed et al. 1994). Ethyl cyanoacetate (**2**) was bought from Aldrich (St. Louis, MO, USA).

Reactions of 4-hydroxy-2-oxo-quinoline-3-carbaldehydes 4a-g with ethyl cyanoacetate (2)

Synthesis of pyrano[3,2-c]quinoline-3-carboxylates 3a-j.

Method I A mixture of **4a-j** (1 mmol), and ethyl cyanoacetate (**2**, 1 mmol, 0.113 g) in 25 mL absolute ethanol and a catalytic amount of piperidine (0.5 mL) was stirred at room temperature for 16–26 h. The reaction was monitored by TLC analysis. The formed products **3a-j** were filtered off and washed with ethanol (30 mL). The obtained products were recrystallized from the stated solvents to afford pure pyrano[3,2-c]quinoline-3-carboxylates **3a-j**.

Method (II) The same above method was repeated by exposing the reaction mixture to MW irradiation in Milestone Microwave Labstation. All the reactions between **4a-j** and **2** were monitored during 5–10 min by TLC using ethyl acetate:petroleum ether (1:1) as an eluent and were carried out until starting materials were completely consumed. After the reaction was completed, the formed products **3a-j** were filtered off, washed with ethanol (30 mL) and were recrystallized from the stated solvents.

Ethyl 2,5-dioxo-5,6-dihydro-2H-pyrano[3,2-c]quinoline-3-carboxylate (3a): Yellow crystals (EtOH); yield: 0.242 g (85%); m.p. = 305 °C (lit 305 °C; Schmidt and Junek 1978). ^{1}H NMR (400 MHz, DMSO-d_6): δ_H = 12.32 (s, 1H, NH), 8.65 (s, 1H, Ar–H), 8.01 (d, J = 7.8 Hz, 1H, Ar–H), 7.73–7.71 (m, 1H, Ar–H), 7.40–7.38 (dd, 2H, Ar–H), 4.31 (q, J = 7.1 Hz, 2H, CH_2-ester), 1.32 (t, J = 7.1 Hz, 3H, CH_3-ester). ^{13}C NMR (100 MHz, DMSO-d_6): δ_C = 163.9 (C=O) 161.8 (C=O), 159.1 (C=O), 155.3 (Cq, Ar–C), 145.8 (Cq, Ar–C), 140.4 (+, Ar–CH), 134.7 (+, Ar–CH), 123.2 (+, 2xAr–CH), 116.4 (Cq, Ar–C), 114.9 (Cq, Ar–C), 111.5 (+, Ar–CH), 107.4 (Cq, Ar–C), 61.2 (−, CH_2), 14.0 (+, CH_3). IR (KBr): ν_{max}/cm^{-1} = 3162 (NH), 3010 (CH-Ar), 2963 (CH-Aliph), 1772 (C=O, Pyranone), 1695 (C=O, Ester), 1664 (C=O, Quinolone). MS (Fab, 70 eV, %): m/z = 286 (45) [M+H]$^+$. *Anal. Calcd. for* $C_{15}H_{11}NO_5$ (285.26): C, 63.16; H, 3.89; N, 4.91. *Found*: C, 63.18; H, 3.86; N, 4.90.

Ethyl 6-methyl-2,5-dioxo-5,6-dihydro-2H-pyrano[3,2-c] quinoline-3-carboxylate (3b): Yellow crystals (CH$_3$OH); yield: 0.263 g (88%); m.p. 286–288 °C (lit 286–288 °C; Morsy et al. 2016). ^{1}H NMR (400 MHz, DMSO-d_6): δ_H = 8.69 (s, 1H, Ar–H), 8.12 (dd, J = 8.0, 1.4 Hz, 1H, Ar–H), 7.91–7.84 (m, 1H, Ar–H), 7.69 (d, J = 8.6 Hz, 1H, Ar–H), 7.46 (dd, J = 8.0, 7.3 Hz, 1H, Ar–H), 4.32 (q, J = 7.1 Hz, 2H, CH_2), 3.69 (s, 3H, CH_3), 1.33 (t, J = 7.1 Hz, 3H, CH_3). ^{13}C NMR (100 MHz, DMSO-d_6): δ_C = 163.8 (C=O), 162.1 (C=O), 160.8 (C=O), 158.3 (Cq, Ar–C), 146.2 (Cq, Ar–C), 140.8 (+, Ar–CH), 134.8 (+, Ar–CH), 123.8 (+, Ar–CH), 123.3 (+, Ar–CH), 116.1 (Cq, Ar–C),

115.4 (Cq, Ar–C), 112.2 (+, Ar–CH), 106.7 (Cq, Ar–C), 61.3 (−, CH_2), 29.7 (+, CH_3), 14.1 (+, CH_3). IR (KBr): ν_{max}/cm^{-1} = 3056 (CH-Ar), 2979 (CH-Aliph), 1769 (C=O, Pyranone), 1690 (C=O, Ester), 1658 (C=O, Quinolone), 1468 (CH$_2$), 1375 (CH$_3$). *Anal. Calcd. for* $C_{16}H_{13}NO_5$ (299.28): C, 64.21; H, 4.38; N, 4.68. Found: C, 64.00; H, 4.20; N, 4.50.

Ethyl 9-methoxy-2,5-dioxo-5,6-dihydro-2H-pyrano[3,2-c]quinoline-3-carboxylate (3c): Yellow crystals (EtOH); Yield: 0.274 g (87%); m.p. 270–272 °C (EtOH). ^{1}H NMR (400 MHz, DMSO-d_6, ppm): δ_H = 12.16 (s, 1H, NH), 8.65 (s, 1H, Ar–H), 7.46–7.24 (m, 3H, Ar–H), 4.30 (q, J = 7.1 Hz, 2H, CH_2), 3.87 (s, 3H, CH_3O), 1.32 (t, J = 7.1 Hz, 3H, CH_3). ^{13}C NMR (100 MHz, DMSO-d_6, ppm): δ_C = 161.9 (C=O), 161.4 (C=O), 158.3(C=O), 155.0 (C$_q$, Ar–C), 154.8 (C$_q$, Ar–C), 145.7 (+, Ar–CH), 135.0 (C$_q$, Ar–C), 124.6 (C$_q$, Ar–C), 118.0 (C$_q$, Ar–C), 114.7 (+, Ar–CH), 111.6 (+, Ar–CH), 107.6 (C$_q$, Ar–C), 103.1 (+, Ar–CH), 61.2 (−, CH_2), 55.7 (+, CH_3O), 14.0 (+, CH_3). IR (KBr): ν_{max}/cm^{-1} = 3276 (NH), 3076 (CH-Ar), 1766 (C=O, Pyranone), 1671 (C=O, Ester), 1604 (C=O, Quinolone), 1458 (CH$_2$), 1370 (CH$_3$), 1347 (OCH$_3$). MS (FAB, 3-NBA), m/z (%): 316 (22) [M+H]$^+$, 315 (10) [M]$^+$. *Anal. Calcd. for* $C_{16}H_{13}NO_6$ (315.28): C, 60.95; H, 4.16; N, 4.44. *Found*: C, 60.93; H, 4.19; N, 4.42.

Ethyl 6-ethyl-2,5-dioxo-5,6-dihydro-2H-pyrano[3,2-c]quinoline-3-carboxylate (3d): Yellow crystals (DMF/EtOH); yield: 0.269 g (86%), m.p. 250–252 °C. ^{1}H NMR (400 MHz, DMSO-d_6, ppm): δ_H = 8.70 (s, 1H, Ar–H), 8.14 (dd, J = 8.0, 1.5 Hz, 1H, Ar–H), 7.92–7.83 (m, 1H, Ar–H), 7.76 (d, J = 8.6 Hz, 1H, Ar–H), 7.45 (t, J = 7.6 Hz, 1H, Ar–H), 4.40–4.26 (m, 4H, 2xCH_2), 1.32 (t, J = 7.1 Hz, 3H, CH_3), 1.25 (t, J = 7.0 Hz, 3H, CH_3). ^{13}C NMR (100 MHz, DMSO-d_6, ppm): δ_C = 162.0 (C=O), 160.7 (C=O), 158.0 (C=O), 154.9 (Cq, Ar–C), 146.1 (C$_q$, Ar–C), 139.8 (+, Ar–CH), 134.9 (+, Ar–CH), 124.1 (+, Ar–CH), 123.2 (+, Ar–CH), 115.7 (C$_q$, Ar–C), 115.3 (C$_q$, Ar–C), 112.3 (Cq, Ar–C), 106.7 (+, Ar–CH), 61.3 (−, CH_2), 37.2 (−, CH_2), 14.0 (+, CH_3), 12.6 (+, CH_3). IR (KBr): ν_{max}/cm^{-1} = 3034 (CH-Ar), 2967 (CH-Aliph), 1750 (C=O, pyranone), 1709 (C=O, Ester), 1653 (C=O, Quinolone), 1463 (CH$_2$), 1373 (CH$_3$). MS (FAB, 3-NBA), m/z (%): 313.1 (25) [M]$^+$, 314.1 (100) [M+H]$^+$. *Anal. Calcd. for* $C_{17}H_{15}NO_5$ (313.31): C, 65.17; H, 4.83; N, 4.47. *Found*: C, 65.19; H, 4.80; N, 4.44.

Ethyl 8-chloro-2,5-dioxo-5,6-dihydro-2H-pyrano[3,2-c] quinoline-3-carboxylate (3e): Yellow crystals (CH$_3$OH); yield: 0.300 g (94%); m.p. 290–292 °C. ^{1}H NMR (400 MHz, DMSO-d_6, ppm): δ_H = 12.42 (s, 1H, NH-isomer1), 12.28 (s, 1H, NH-isomer2), 8.66 (d, J = 7.1 Hz, 1H, Ar–H-isomer1), 8.60 (d, J = 6.3 Hz, 1H, Ar–H-isomer2), 8.00 (d, J = 8.5 Hz, 1H, Ar–H-isomer1), 7.65 (t, J = 8.1 Hz, 1H, Ar–H-isomer2), 7.38 (ddd, J = 10.5, 6.2, 2.8 Hz, 4H, Ar–H-isomer1 + -isomer2), 4.23–4.17 (m, 4H, CH_2-isomer1 and isomer2), 1.31 (t, J = 7.1 Hz, 6H, CH_3 isomer1 + -isomer2). ^{13}C

NMR (100 MHz, DMSO-d_6, ppm): δ_C = 161.9 (C=O), 161.6 (C=O), 158.8 (C=O), 154.7 (Cq, Ar–C), 145.3 (Cq, Ar–C), 142.3 (+, Ar–CH), 138.8 (Cq, Ar–C), 130.5 (+, Ar–CH), 125.4 (+, Ar–CH), 115.8 (Cq, Ar–C), 115.2 (Cq, Ar–C), 110.3 (Cq, Ar–C), 108.5 (+, Ar–CH), 61.3 (–, CH$_2$-isomer1 + -isomer2), 14.0 (+, CH$_3$-isomer1 + -isomer2). Other isomer: 161.8 (C=O), 161.4 (C=O), 158.3 (C=O), 154.5 (Cq, Ar–C), 145.2 (Cq, Ar–C), 140.8 (+, Ar–CH), 134.0 (Cq, Ar–C), 126.0 (+, Ar–CH), 123.3 (+, Ar–CH), 115.5 (Cq, Ar–C), 114.8 (Cq, Ar–C), 109.1 (Cq, Ar–C), 107.5 (+, Ar–CH). IR (KBr) ν_{max}/cm^{-1} = 3268(NH), 3056 (CH-Ar), 2853 (CH-Aliph), 1775 (C=O, Pyranone), 1663 (C=O, Ester), 1598 (C=O, Quinolone,), 1475 (CH$_2$), 1361(CH$_3$). MS (FAB, 3-NBA), m/z (%): 320/321 (100/23) [M]$^+$, 274/275 (55/11), 155/154 (21/82). Anal. Calcd. for C$_{15}$H$_{10}$ClNO$_5$ (319.70): C, 56.35; H, 3.15; Cl, 11.09; N, 4.38. Found: C, 56.33; H, 3.17; Cl, 11.11; N, 4.36.

Ethyl 8-methyl-2,5-dioxo-5,6-dihydro-2H-pyrano[3,2-c]quinoline-3-carboxylate (3f): Yellow crystals (EtOH); yield: 0.260 g (87%); m.p 232–234 °C (EtOH). ^{1}H NMR (400 MHz, DMSO-d_6, ppm): δ_H = 12.16 (d, J = 12.0 Hz, 2H, NH-isomer1 + -isomer2), 8.66 (dd, J = 19.6, 2.4 Hz, 2H, Ar–H-isomer1 + -isomer2), 7.89 (d, J = 8.5 Hz, 2H, Ar–H-isomer1), 7.58 (t, J = 7.8 Hz, 1H, Ar–H-isomer2), 7.29–7.12 (m, 4H, Ar–H-isomer1 + -isomer2), 4.30 (qd, J = 7.1, 3.2 Hz, 4H, CH$_2$-isomer1 + -isomer2), 2.81 (s, 3H, CH$_3$ isomer1), 2.43 (s, 3H, CH$_3$ isomer2), 1.32 (td, J = 7.1, 1.1 Hz, 6H, CH$_3$ isomer1 + -isomer2). ^{13}C NMR (100 MHz, DMSO-d_6, ppm): δ_C = 164.3 (C=O), 163.8 (C=O), 162.0 (C=O), 158.6 (Cq, Ar–C), 155.0 (Cq, Ar–C), 145.6 (+, Ar–CH), 140.4 (Cq, Ar–C), 133.8 (+, Ar–CH), 124.7 (+, Ar–CH), 115.9 (Cq, Ar–C), 114.1 (Cq, Ar–C), 110.6 (Cq, Ar–C), 107.6 (+, Ar–CH), 61.2 (–, CH$_2$-isomer1 + -isomer2), 23.2 (+, CH$_3$-isomer1), 14.1 (+, CH$_3$-isomer1 + -isomer2), 163.9 (C=O), 162.2 (C=O), 159.0 (C=O), 155.1 (Cq, Ar–C), 145.8 (Cq, Ar–C), 141.5 (+, Ar–CH), 137.6 (Cq, Ar–C), 126.1 (+, Ar–CH), 123.2 (+, Ar–CH), 114.7 (Cq, Ar–C), 113.5 (Cq, Ar–C), 109.2 (Cq, Ar–C), 106.7 (+, Ar–CH), 21.7 (+, CH$_3$-isomer2). IR (KBr): ν_{max}/cm^{-1} = 3176 (NH), 3065 (CH-Ar), 2967 (CH-Aliph), 1774 (C=O, Pyranone), 1658 (C=O, Ester), 1607 (C=O, Quinolone), 1490 (CH$_2$), 1363 (CH$_3$). MS (Fab, 70 eV, %): m/z = 299 (20) [M]$^+$, 300 (100) [M+H]$^+$, 254 (61), 154 (62). Anal. Calcd. for C$_{16}$H$_{13}$NO$_5$ (299.28): C, 64.21; H, 4.38; N, 4.68. Found: C, 64.23; H, 4.36; N, 4.66.

Ethyl 9-bromo-2,5-dioxo-5,6-dihydro-2H-pyrano[3,2-c]quinoline-3-carboxylate (3g): Yellow crystals (DMF/MeOH); yield: 0.349 g (96%); m.p. 330–332 °C. ^{1}H NMR (400 MHz, DMSO-d_6, ppm): δ_H = 12.37 (s, 1H, NH), 8.62 (s, 1H, Ar–H), 8.07 (d, J = 2.1 Hz, 1H, Ar–H), 7.90 (dd, J = 8.8, 2.2 Hz, 1H, Ar–H), 7.37 (d, J = 8.9 Hz, 1H, Ar–H), 4.31 (q, J = 7.1 Hz, 2H, CH$_2$), 1.32 (t, J = 7.1 Hz, 3H, CH$_3$). IR (KBr) ν_{max}/cm^{-1} = 3268 (NH), 3056 (CH-Ar), 2828 (CH-Aliph),

1767 (C=O, Pyranone), 1655 (C=O, Ester), 1541 (C=O, Quinolone), 1485(CH$_2$), 1375 (CH$_3$). MS (Fab, 70 eV, %): m/z = 365/366 (75/32) [M]$^+$, 317/318 (30/35). Anal. Calcd. for C$_{15}$H$_{10}$BrNO$_5$ (364.15): C, 65.17; H, 4.83; N, 4.47. Found: C, 65.21; H, 4.78; N, 4.42.

Ethyl 9-chloro-2,5-dioxo-5,6-dihydro-2H-pyrano[3,2-c]quinoline-3-carboxylate (3h): Yellow crystals (EtOH); yield: 0.301 g (94%); m.p. 274–276 °C (EtOH). ^{1}H NMR (400 MHz, DMSO-d_6, ppm): δ_H = 12.32 (s, 1H, NH), 8.59 (s, 1H, Ar–H), 7.89 (d, J = 2.3 Hz, 1H, Ar–H), 7.76 (dd, J = 8.9, 2.4 Hz, 1H, Ar–H), 7.38 (d, J = 8.9 Hz, 1H, Ar–H), 4.30 (q, J = 7.1 Hz, 2H, CH$_2$), 1.32 (t, J = 7.1 Hz, 3H, CH$_3$). ^{13}C NMR (100 MHz, DMSO-d_6, ppm): δ_C = 161.8 (C=O), 160.7 (C=O), 158.6 (C=O), 154.7 (Cq, Ar–C), 145.2 (+, Ar–CH), 138.8 (Cq, Ar–C), 134.2 (Cq, Ar–C), 127.1 (Cq, Ar–C), 122.1 (Cq, Ar–C), 118.4 (+, Ar–CH), 115.6 (+, Ar–CH), 112.5 (Cq, Ar–C), 108.0 (+, Ar–CH), 61.4 (–, CH$_2$), 14.0 (+, CH$_3$). IR (KBr): ν_{max}/cm^{-1} = 3270 (NH), 3058 (CH-Ar), 2891 (CH-Aliph), 1769 (C=O, Pyranone), 1690 (C=O, ester), 1660 (C=O, quinolone), 1490 (CH$_2$), 1363 (CH$_3$). MS (FAB, 3-NBA), m/z (%): 319/320 (4/21) [M]$^+$, 154/155 (100/30), 137/138 (70/38). Anal. Calcd. for C$_{15}$H$_{10}$ClNO$_5$ (319.70): C, 64.21; H, 4.38; N, 4.68. Found: C, 64.23; H, 4.36; N, 4.66.

Ethyl 9-flouro-2,5-dioxo-5,6-dihydro-2H-pyrano[3,2-c]quinoline-3-carboxylate (3i): Yellow crystals (EtOH); yield: 0.278 g (92%); m.p. 292–294 °C (EtOH). ^{1}H NMR (400 MHz, DMSO-d_6, ppm): δ_H = 12.30 (s, 1H, NH), 8.63 (s, 1H, Ar–H), 7.74 (dd, J = 2.8 Hz, J = 8.8 Hz, 1H, Ar–H), 7.67–7.65 (m, 1H, Ar–H), 7.44 (dd, J = 4.5 Hz, J = 9.1 Hz, 1H, Ar–H), 4.31 (q, J = 7.1 Hz, 2H, CH$_2$), 1.32 (t, J = 7.1 Hz, 3H, CH$_3$). ^{13}C NMR (100 MHz, DMSO-d_6, ppm): δ_C = 161.9 (C=O), 161.2 (C=O), 158.6 (C=O), 156.2 (Cq, Ar–C), 154.8 (Cq, Ar–C), 145.3 (Cq, Ar–C), 136.9 (Cq, Ar–C), 122.7 (+, Ar–CH), 118.6 (+, Ar–CH), 115.6 (Cq, Ar–C), 112.1 (+, Ar–CH), 108.3 (Cq, Ar–C), 108.1 (+, Ar–CH), 61.4 (–, CH$_2$), 14.0 (+, CH$_3$). IR (KBr): ν_{max}/cm^{-1} = 3195 (NH), 3060 (CH-Ar), 2990 (CH-Aliph), 1729 (C=O, Pyranone), 1660 (C=O, Ester), 1649 (C=O, Quinolone), 1470 (CH$_2$), 1365 (CH$_3$). MS (FAB, 3-NBA), m/z (%): 303/304 (8/37) [M]$^+$, 289/290 (20/6), 258/259 (11/2), 154/155 (100/30). Anal. Calcd. for C$_{15}$H$_{10}$FNO$_5$ (303.25): C, 59.41; H, 3.32; N, 4.62. Found: C, 59.43; H, 3.35; N, 4.60.

Ethyl 9-methyl-2,5-dioxo-5,6-dihydro-2H-pyrano[3,2-c]quinoline-3-carboxylate (3j): Yellow crystals (DMF/EtOH); yield: 0.260 g (87%); m.p. 276–278 °C. ^{1}H NMR (400 MHz, DMSO-d_6, ppm): δ_H = 12.13 (s, 1H, NH), 8.63 (s, 1H, Ar–H), 7.77 (s, 1H, Ar–H), 7.55 (dd, J = 1.6 Hz, J = 8.7 Hz, 1H, Ar–H), 7.29 (d, J = 8.6 Hz, 1H, Ar–H), 4.30 (q, J = 7.1 Hz, 2H, CH$_2$), 2.40 (s, 3H, CH$_3$),1.32 (t, J = 7.1 Hz, 3H, CH$_3$). IR (KBr): ν_{max}/cm^{-1} = 3160 (NH), 3063 (CH-Ar), 2980 (CH-Aliph), 1769 (C=O, Pyranone), 1699 (C=O, Ester), (1608, C=O, Quinolone), 1507 (CH$_2$),

1366 (CH$_3$). MS (FAB, 3-NBA), *m/z* (%): 300 [M + 1] (52), 299 [M]$^+$ (16), 154 (100), 137 (69), 136 (63). *Anal. Calcd. for* C$_{16}$H$_{13}$NO$_5$ (299.28): C, 64.21; H, 4.38; N, 4.68. *Found*: C, 64.23; H, 4.36; N, 4.70.

Single Crystal X-ray structure analysis

Single crystal X-ray diffraction data of **3b** were collected on a STOE STADIVARI diffractometer with monochromated Ga Kα (1.34143 Å) radiation at 180 K. Using Olex2 (Dolomanov et al. 2009), the structures were solved with the ShelXT (Sheldrick *SHELXT* 2015) structure solution program using Intrinsic Phasing and refined with the ShelXL (Sheldrick 2015a, b) refinement package using Least Squares minimization. Refinement was performed with anisotropic temperature factors for all non-hydrogen atoms; hydrogen atoms were calculated on idealized positions. SI Table 1 in the supplement summarizes crystal and refinement data of **3b**.

Crystallographic data of compound **3b** reported in this paper have been deposited with the Cambridge Crystallographic Data Centre as supplementary information no. CCDC-2252172. Copies of the data can be obtained free of charge from https://www.ccdc.cam.ac.uk/structures/.

Computational methodology

The X-ray resolved structures of the EGFR and BRAF^{V600E} with PDB IDs: 1M17 (Stamos et al. 2002) and 3OG7 (Bollag et al. 2010), were downloaded and used as templates for all in silico computations. For the preparation of the PDB files, all ions, ligands, water molecules, and heteroatoms were eliminated. All missing residues were constructed using Modeller software (Marti-Renom et al. 2000). At pH 7.0, the investigated targets' titratable residues were examined using the empirical program PropKa to determine their protonation states (Olsson et al. 2011). Omega2 software was used to model the 3D structures of compounds **3c**, **3g**, and **3h** (Hawkins et al 2010; OMEGA 2013). Using the MMFF94S force field integrated into the SZYBKI software, the generated structures were energetically minimized (Halgren TA 1999, SZYBKI 2016).

All docking calculations were carried out using the AutoDock4.2.6 software (Morris et al. 2009). The grid map of 50 Å × 50 Å × 50 Å was positioned at the center of the binding pockets of the EGFR and BRAF^{V600E} proteins with a spacing of 0.375 Å. Lamarckian genetic algorithm was employed with the following parameters: a maximum number of 25,000,000 energy evaluations, 250 independent docking runs, an initial population of 300, and a maximum number of 27,000 generations. The atomic charges of these compounds were assigned using the Gasteiger-Marsili method (Gasteiger J and Marsili M 1980). The Discovery Studio module of the Biovia software was used to show all molecular interactions (Dassault Systèmes BIOVIA: San Diego, CA, USA, 2019).

Conclusion

Owing to the importance of pyrano[3,2-*c*]quinoline derivatives, we direct for the synthesis of pyrano[3,2-*c*]quinoline-3-carboxylates **3a-j** from the microwave assisted the reaction of 4-hydroxy-2-oxo-1,2-dihydroquinoline-3-carbaldehydes **4a-j** with ethyl cyanoacetate (**2**). The structure of compounds was examined by NMR spectroscopy and elemental analyses in addition to X-ray structure analysis. The newly synthesized compounds were evaluated for their in vitro antiproliferative activity against four cancer cell lines. Compounds **3a-j** were tested for antiproliferative activity against four human cancer cell lines using the MTT assay and doxorubicin as the reference drug: pancreas (Panc-1) cancer cell line, breast cancer (MCF-7) cell line, colon cancer (HT-29) cell line, and epithelial cancer (A-549) cell line. The most effective derivatives were compounds **3c**, **3g**, **3h**, and **3i**, with GI$_{50}$ values ranging from 1.30 to 2.20 μM. The most potent antiproliferative derivative, compound **3c** (R^1 = OCH$_3$, R^2 = R^3 = H), was also the most potent EGFR inhibitor, with an IC$_{50}$ value of 105 ± 08 nM, 1.3-fold less potent than erlotinib (IC$_{50}$ = 80 ± 05 nM). Ultimately, the findings of the docking study demonstrated that all of the examined inhibitors had favorable docking scores against the EGFR and BRAF^{V600E}.

Declarations

Conflict of interest The authors declare no conflict of interest.

References

Abdelrahman MH, Aboraia HS, Youssif BGM, Elsadek BEM (2017) Design, synthesis and pharmacophoric model building of new 3-alkoxy-methyl/3-phenyl indole-2-carboxamides with potential antiproliferative activity. Chem Biol Drug Des 90:64–821

Aghbash KO, Pesyan NN (2022) Anchoring of nickel (II) kojic acid in functionalized Si-MCM-41 matrix: a effective nanocatalyst for the catalytic clean synthesis of dihydropyrano[3,2-*b*]

chromenediones. J Iran Chem Soc 19:1467–1479. https://doi.org/10.1007/s13738-021-02395-6

Aghbash KO, Pesyan NN, Notash B (2018) The clean synthesis and confirmatory structural characterization of new 2-amino-4,8-dihydropyrano[3,2-*b*]pyran-3-cyano based on Kojic acid. Monatsh Chem 149:2059–2067. https://doi.org/10.1007/s00706-018-2254-3

Aghbash KO, Pesyan NN, Şahin E (2019a) Cu(I)-catalyzed alkyne–azide 'click' cycloaddition (CuAAC): a clean, efficient, and mild synthesis of new 1,4-disubstituted 1*H*–1,2,3-triazole-linked 2-amino-4,8-dihydropyrano[3,2-b]pyran-3-carbonitrile–crystal structure. Res Chem Intermed 45:2079–2094. https://doi.org/10.1007/s11164-018-03723-x

Aghbash KO, Pesyan NN, Batmani H (2019b) Fe3O4@silica-MCM-41@DABCO: A novel magnetically reusable nano-structured catalyst for clean *in situ* synthesis of substituted 2-aminodihydropyrano[3,2-*b*]pyran-3-cyano. Appl Organometall Chem 33(11):5227. https://doi.org/10.1002/aoc.5227

Aly AA, El-Sheref EM, Bakheet MEM, Mourad MAE, Bräse S, Ibrahim MAA, Nieger M, Garvalov BK, Dalby KN, Kaoud TS (2019) Design, synthesis and biological evaluation of fused naphthofuro[3,2-*c*]quinoline-6,7,12-triones and pyrano[3,2-c]quinoline-6,7,8,13-tetraones derivatives as ERK inhibitors with efficacy in BRAF-mutant melanoma. Bioorg Chem. 82:290–305

Al-Yahya MA, Al-Rehaily AJ, Ahmed MS, Al-Said MS, El-Feraly FS, Hufford CD (1992) New alkaloids from *Haplophyllum tuberculatum*. J Nat Prod 55:899–903. https://doi.org/10.1021/np50085a008

Badiger KB, Sannegowda LK, Kamanna K (2022) Microwave-assisted one-pot synthesis of tetrahydrobenzo[*b*]pyrans in the presence of WEWFPA and their electrochemical studies. Org Commun 15:148–166

Beigiazaraghbelagh P, Poursattar Marjani A (2024) Carbon-based catalysts: advances in synthesizing *N*-heterocyclic compounds using graphene family and graphite oxide. Res Chem Intermed 50:485–531. https://doi.org/10.1007/s11164-023-05205-1

Bhudevi B, Ramana PV, Mudiraj A, Reddy AR (2009) Synthesis of 4-hydroxy-3-formylideneamino-l*H*/methyl/phenylquinolin-2-ones. Indian J Chem B 48:255–260

Bibak S, Poursattar Marjani A (2023) Magnetically retrievable nanocatalyst Fe$_3$O$_4$@CPTMO@dithizone-Ni for the fabrication of 4*H*-benzo[*h*]chromenes under green medium. Sci Rep 13:17894. https://doi.org/10.1038/s41598-023-44881-2

Biovia DS, Bdsv V (2019) Dassault Systèmes BIOVIA: San Diego. CA, USA

Bollag G, Hirth P, Tsai J, Zhang J, Ibrahim PN, Cho H, Spevak W, Zhang C, Zhang Y, Habets G, Burton EA, Wong B, Tsang G, West BL, Powell B, Shellooe R, Marimuthu A, Nguyen H, Zhang KYJ, Artis DR, Schlessinger J, Su F, Higgins B, Iyer R, D'Andrea K, Koehler A, Stumm M, Lin PS, Lee RJ, Grippo J, Puzanov I, Kim KB, Ribas A, McArthur GA, Sosman JA, Chapman PB, Flaherty KT, Xu X, Nathanson KL, Nolop K (2010) Clinical efficacy of a RAF inhibitor needs broad target blockade in BRAF-mutant melanoma. Nature 467:596–599

Buckle DR, Cantello BCC, Smith H, Spicer BA (1975) 4-Hydroxy-3-nitro-2-quinolones and related compounds as inhibitors of allergic reactions. J Med Chem 18:726–732

Chen I-S, Wu S-J, Tsai I-L, Wu T-S, Pezzuto JM, Lu MC, Chai H, Suh N, Teng C-M (1994) Chemical and bioactive constituents from *Zanthoxylum simulan*s. J Nat Prod 57:1206–1211. https://doi.org/10.1021/np50111a003

Di Liberto MG, Caldo AJ, Quiroga AD, Riveira MJ, Derita MG (2020) Zanthosimuline and related pyranoquinolines as antifungal agents for postharvest fruit disease control. ACS Omega 5(13):7481–748

Dolomanov OV, Bourhis LJ, Gildea RJ, Howard JAK, Puschmann H (2009) OLEX2: a complete structure solution, refinement and analysis program. J Appl Cryst 42:339–341

Duraipandiyan V, Ignacimuthu S (2009) Antibacterial and antifungal activity of Flindersine isolated from the traditional medicinal plant Toddalia asiatica (L.) Lam. J Ethnopharm 123:494–498

Ea S, Giacometti S, Ciccolini J, Akhmedjanova V, Aubert C (2008) Cytotoxic effects of haplamine and its major metabolites on human cancer cell lines. Planta Med 74(10):1265–8

Elbastawesy MAI, Aly AA, Ramadan M, Elshaier YAMM, Youssif BGM, Brown AB, Abuo-Rahma GEl-Din A (2019) Novel pyrazoloquinolin-2-ones: design, synthesis, docking studies, and biological evaluation as antiproliferative EGFR-TK inhibitors. Bioorg Chem 90:103045

Elbastawesy MAI, Aly AA, El-Shaier YAMM, Brown AB, Abuo-Rahma GE-DA, Ramadan M (2021) New 4-thiazolidinone/quinolin-2-ones scaffold: design, synthesis, docking studies and biological evaluation as potential urease inhibitors. J Mol Struct 1244:130845. https://doi.org/10.1016/j.molstruc.2021.130845

Elshaier YAMM, Aly AA, Abdel-Aziz M, Fathy HM, Brown AB, Bräse S, Ramadan M (2022) Synthesis and identification of new N, N-disubstituted thiourea, and thiazolidinone scaffolds based on quinolone moiety as urease inhibitor. Molecules 27:7126

El-Sherief HAM, Youssif BGM, Bukhari SNA, Abdel-Aziz M, Abdel-Rahman HM (2018) Novel 1,2,4-triazole derivatives as potential anticancer agents: design, synthesis, molecular docking, and mechanistic studies. Bioorg Chem 76:314–325

Gasteiger J, Marsili M (1980) Iterative partial equalization of orbital electronegativity–a rapid access to atomic charges. Tetrahedron 36:3219–3228

Halgren TA (1999) MMFF VI. MMFF94s option for energy minimization studies. J Comput Chem 20:720–729

Hawkins PCD, Skillman AG, Warren GL, Ellingson BA, Stahl MT (2010) Conformer generation with OMEGA: algorithm and validation using high quality structures from the protein databank and cambridge structural database. J Chem Inf Model 50:572–584

Ho C-C, Liao W-Y, Lin C-A, Shih J-Y, Yu C-J, Yang JC-H (2017) Acquired BRAF V600E mutation as resistant mechanism after treatment with osimertinib. J Thorac Oncol 12:567–572. https://doi.org/10.1016/j.jtho.2016.11.2231

Hyman DM, Puzanov I, Subbiah V, Faris JE, Chau I, Blay J-Y, Wolf J, Raje NS, Diamond EL, Hollebecque A, Gervais R, Elez-Fernandez ME, Italiano A, Hofheinz R-D, Hidalgo M, Chan E, Schuler M, Lasserre SF, Makrutzki M, Sirzen F, Veronese ML, Tabernero J, Baselga J (2015) Vemurafenib in multiple nonmelanoma cancers with BRAF V600 mutations. New Engl J Med 373:726–736. https://doi.org/10.1056/NEJMoa1502309

Insuasty D, Vidal O, Bernal A, Marquez E, Guzman J, Insuasty B, Quiroga J, Svetaz L, Zacchino S, Puerto G, Abonia R (2019) Antimicrobial activity of quinoline-based hydroxyimidazolium hybrids. Antibiotics (Basel) 8(4):239

Ito C, Itoigawa M, Furukawa A, Hirano T, Murata T, Kaneda N, Hisada Y, Okuda K, Furukawa H (2004) Quinolone alkaloids with nitric oxide production inhibitory activity from *Orixa japonica*. J Nat Prod 67:1800–1803. https://doi.org/10.1021/np0401462

Kalla AM, Devaraju R (2017) Microwave energy and its application in food industry: a review. Asian J Dairy Food Res. 36:37–44

Kappe CO (2004) Controlled microwave heating in modern organic synthesis. Angew Chem Int Ed 43:6250–6284

Magedov IV, Manpadi M, Ogasawara MA, Dhawan AS, Rogelj S, Van Slambrouck S, Steelant WFA, Evdokimov NM, Uglinskii PY, Elias EM, Knee EJ, Tongwa P, Antipin MY, Kornienko A (2008) Structural simplification of bioactive natural products with multicomponent synthesis. 2. Antiproliferative and antitubulin activities of pyrano[3,2-c]pyridones and pyrano[3,2-c]quinolones. J Med Chem 51(8):2561–2570

Mahmoud MA, Mohammed AF, Salem OIA, Gomaa HAM, Youssif BGM (2022) New 1,3,4-oxadiazoles linked 1,2,3-triazole moiety as antiproliferative agents targeting the EGFR tyrosine kinase. Arch Pharm 355:2200009

Marti-Renom MA, Stuart AC, Fiser A, Sanchez R, Melo F, Sali A (2000) Comparative protein structure modeling of genes and genomes. Ann Rev Biophys Biomol Struct 29:291–325

Maynard R (2005) Indoor environment: airborne particles and settled dust. Appl Organomet Chem 19(1):215–215. https://doi.org/10.1002/aoc.724

Mohamed EA, Ismail MM, Gabr Y, Abass M (1994) Synthesis of some multiazaheterocycles as substituents to quinolone moiety of specific biological activity. Chem Pap 48:285–292

Mohamed FAM, Gomaa HAM, Hendawy OM, Ali AT, Farghaly HS, Gouda AM, Abdelazeem AH, Abdelrahman MH, Trembleau L, Youssif BGM (2021) Design, synthesis, and biological evaluation of novel EGFR inhibitors containing 5-chloro-3-hydroxymethyl-indole-2-carboxamide scaffold with apoptotic antiproliferative activity. Bioorg Chem 112:104960

Mohassab AM, Hassan HA, Abdelhamid D, Gouda AM, Youssif BGM, Tateishi H, Fujita M, Otsuka M, Abdel-Aziz M (2021) Design and synthesis of novel quinoline/chalcone/1,2,4-triazole hybrids as potent antiproliferative agent targeting EGFR and BRAF^{V600E} kinases. Bioorg Chem 106:104510

Morris GM, Huey R, Lindstrom W, Sanner MF, Belew RK, Goodsell DS, Olson AJ (2009) AutoDock4 and AutoDockTools4: Automated docking with selective receptor flexibility. J Comput Chem 30:2785–2791

Morsy JM, Hassanin HM, Ismail MM, Abd-Alrazk MMA (2016) Synthesis of new quinolinones from 3-nitropyranoquinolinones. J Chem Res 40:239–246

Moynihan E, Mackey K, Blaskovich MAT, Reen FJ, McGlacken G (2022) N-Alkyl-2-quinolonopyrones demonstrate antimicrobial activity against ESKAPE pathogens including Staphylococcus aureus. ACS Med Chem Lett 13:1358–1362

Ohlsson T, Bengtsson N (2001) Microwave technology and foods. Adv Food Nutr Res 43:65–140

Olsson MHM, Sondergaard CR, Rostkowski M, Jensen JH (2011) PROPKA3: consistent treatment of internal and surface residues in empirical pKa predictions. J Chem Theory Comput 7:525–537

OMEGA 2.5.1.4 (2013) OpenEye Scientific Software: Santa Fe, NM, USA

Pesyan NN, Bardajee GR, Kashani E, Mohammadi M, Batmani H (2020) Ni(II)-Schiff base/SBA-15: a nanostructure and reusable catalyst for one-pot three-component green synthesis of 3,4-dihydropyrano[3,2-c]chromene derivatives. Res Chem Intermed 46:347–367. https://doi.org/10.1007/s11164-019-03954-6

Poursattar Marjani A, Asadzadeh F, Danandeh Asl A (2023) Novel core–shell magnetic nanoparticles@Zeolitic imidazolate with glycerol-nickel for the synthesis of dihydropyrimidinones. Appl Organomet Chem 37(11):e7260

Prasad P, Shobhashana PG, Patel MP (2017) An efficient synthesis of 4H-pyrano quinolinone derivatives catalysed by a versatile organocatalyst tetra-n-butylammonium fluoride and their pharmacological screening. R Soc Open Sci 4(11):170764

Ramadan M, Abd El-Aziz M, Elshaier YAMM, Youssif BGM, Brown AB, Fathy HM, Aly AA (2020) Design and synthesis of new pyranoquinolinone heteroannulated to triazolopyrimidine of potential apoptotic antiproliferative activity. Bioorg Chem 105:104392

Ramadan M, Elshaier YAMM, Aly AA, Abdel-Aziz M, Fathy HM, Brown AB, Pridgen JR, Dalby KN, Kaoud TS (2021) Development of 2′-aminospiro[pyrano[3,2-c]quinoline]-3′-carbonitrile derivatives as non-ATP competitive Src kinase inhibitors that suppress breast cancer cell migration and proliferation. Bioorg Chem 116:105344

Saeed AM, Abdou IM, Salem AA, Ghattas MA, Atatreh N, AlNeyadi SS (2020) Anti-cancer activity and molecular docking of some pyrano[3,2-c]quinoline analogues. Open J Med Chem 10:1–14

Safari E, Poursattar Marjani A, Sadrmohammadi M (2023) Recent progress of nanocatalyst in the synthesis of heterocyclic compounds by barbituric acids. Appl Organometal Chem 37:e7250. https://doi.org/10.1002/aoc.7250

Schmidt HW, Junek H (1978) Syntheses with nitriles, 50: cyclization reactions to pyrano[3,2-c]pyridines and pyrano[3,2-c]quinolines with ethoxymethylenemalono-dinitrile and ethyl cyanoacetate. Monatsh Chem 109:1075–1080

Sheldrick GM (2015a) SHELXT - Integrated space-group and crystal-structure determination. Acta Cryst A 71:3–8. https://doi.org/10.1107/S2053273314026370

Sheldrick GM (2015b) Crystal structure refinement with SHELXL. Acta Cryst C 71:3–8. https://doi.org/10.1107/S20532296140242

Stamos J, Sliwkowski MX, Eigenbrot C (2002) Structure of the epidermal growth factor receptor kinase domain alone and in complex with a 4-anilinoquinazoline inhibitor. J Biol Chem 277:46265–46272

SZYBKI 1.9.0.3 (2016), OpenEye Scientific Software: Santa Fe, NM, USA

Upadhyay KD, Dodia NM, Khunt RC, Chaniara RS, Shah AK (2018) Synthesis and biological screening of pyrano[3,2-c]quinoline analogues as anti-inflammatory and anticancer agents. ACS Med Chem Lett 9(3):283–288. https://doi.org/10.1021/acsmedchemlett.7b00545

Upadhyay DB, Vala RM, Patel SG, Patel PJ, Chi C, Patel HM (2023) Water mediated TBAB catalyzed synthesis of spiro-indoline-pyrano[3,2-c]quinolines as α-amylase inhibitor and in silico studies. J Mol Struct 1273:134305

Win KMN, Sonawane AD, Koketsu M (2019) Iodine mediated in situ generation of R-Se-I: application towards the construction of pyrano[4,3-b]quinoline heterocycles and fluorescence properties. Org Biomol Chem 17:9039–9049

Youssif BGM, Mohamed AM, Osman EEA, Abou-Ghadir OF, Elnaggar DH, Abdelrahman MH, Trembleau L, Gomaa HAM (2019) 5-Chlorobenzo-furan-2-carboxamides: from allosteric CB1 modulators to potential apoptotic antitumor agents. Eur J Med Chem 177:1–11